uc3m | Universidad Carlos III de Madrid

e-Archivo

This is a postprint version of the following published document:

Juste, G. & Fajardo, P. (2018). Influence of flow tree-dimensionality on the heat transfer of a narrow channel backward facing step flows. *International Journal of Thermal Sciences*, vol. 132, pp. 234–248.

DOI: 10.1016/j.ijthermalsci.2018.06.005

© 2018 Elsevier Masson SAS.

This work is licensed under a Creative Commons Attribution-NonCommercial-NoDerivatives 4.0 International License.

Influence of flow tree-dimensionality on the heat transfer of a narrow channel Backward Facing Step flows

Juste, G.L.[a] and Fajardo, P.[b]

[a] Aerospace Propulsion and Fluid Mechanics, Universidad Politécnica de Madrid, Plaza Cardenal Cisneros 3, 28040 Madrid, Spain. E-mail: gregorio.lopez@upm.es
[b] Aerospace Engineering Group. Universidad Carlos III de Madrid, 28911 Leganés, Spain. E-mail: pablo.fajardo@uc3m.es

Abstract

This manuscript studies the forced-mixed convective flow on a three-dimensional backward facing step with low aspect ratio (AR=4) and expansion ratio ER=2 for Reynolds number in the laminar and beginning of transitional regime (Re 100-1200). The analysis is performed using large eddy simulations, with the main objective assessing the effect of sidewalls on heat transfer characteristics on bottom wall in narrow channels with sudden expansion. The numerical model has been validated with experimental and numerical results from the literature and qualitatively with the experimental results obtained through Moiré deflectometry. The bottom surface was kept at constant temperature greater than the flow inlet temperature, while the other walls are considered to be adiabatic. To decouple the three-dimensional flow features due to the sidewalls and the intrinsic three-dimensional instabilities of the separated flow, two different boundary conditions on lateral walls, slip and non-slip, have been used. The results obtained show that when slip sidewalls are considered, the three-dimensional intrinsic structures begging to appear for Re equal to 1200. These structures enhance the heat transfer in the bottom wall. On the contrary, with non-slip sidewalls, the strong three-dimensional structures caused by the sidewalls represented by the upper side recirculation bubble and the wall jets mask the intrinsic three-dimensional instability, decreasing the heat transfer in the lower wall downstream of the step. As a consequence, the surface averaged Nusselt for all Reynolds numbers corresponding to the beginning of the transitional flow is lower for the case of non-slip sidewalls than for the case of slip sidewalls. Thus, the study concludes that sidewalls have a negative effect on heat transfer in narrow channels for flow Reynolds numbers in the early transitional regime.

Keywords

Backward facing step, heat transfer, narrow channels, three-dimensional instabilities.

1. Introduction

Flow separation, with a recirculation region and subsequent reattachment is a common feature encountered in many engineering flows, such as atmospheric flows in contact with the ground surface, ducts with a sudden change in area, airfoils at high angles of attack, and many types of fluid systems used in thermal devices such as turbine blade cooling [1,2], combustion chambers [3,4] and many other applications in all engineering disciplines.

The study presented in this paper is performed on the flow over a backward-facing step (BFS) geometry. This approach is followed for the sake of geometrical simplicity, but keeping the complexity in terms of flow structure and heating transfer features encountered in actual geometries. The fluid flow over a BFS geometry is a well-established case for benchmarking flows with sudden expansions, as the ones of interest in this paper, and it has been the subject of numerous numerical and some experimental studies over the last decades.

Several publications on BFS are focused on laminar, transitional and turbulent adiabatic flows over two-dimensional or three-dimensional geometries with a considerably large aspect ratio, defined as channel width to height ratio upstream of the step, and mainly devoted to characterize the flow structure, reattachment conditions, and other flow features. Some examples can be found in the studies from the literature [5-8].

Following these classical studies, a large number of investigations has been dedicated to improve the understanding the three-dimensional aspects of this flow in the laminar, transitional and turbulent regimes, characterizing the flow behaviour, and mainly focusing on two different phenomena: the effect of the sidewalls on the flow and the three-dimensional stability of the flow over a backward-facing step.

Kaiktsis et al. [9, 10], Barkley et al. [11], Beaudoin et al. [12] amongst others, have carried out detailed analysis on the flow stability from two-dimensional laminar flow to three dimensional flow, obtaining the intrinsically unstable three-dimensional modes, and revealing characteristics such as bifurcation conditions (critical Reynolds number), unsteadiness caused by convective instabilities, or the wavelength of the instabilities.

Concerning the former topic, several investigators have devoted substantial efforts to study the sidewall induced three-dimensionalities in the flow. Williams and Baker [13], Chiang and Sheu [14] and Biswas et al. [15] performed numerical simulations on a BFS with the same aspect ratio used by Armaly et al. [6] for a range of Reynolds numbers in the laminar and near the transitional regimes. The results show the appearance of complex secondary flow patterns near the sidewalls and the development of longitudinal vortices along the channel.

Nie and Armaly [16, 17] and Armaly et al. [18] conducted numerical and experimental studies on three-dimensional BFS geometries with sidewalls a range of expansion ratios (ER) and different Reynolds numbers on a model with an aspect ratio (AR) of 8. The flow features found, include: the development of wall-jets or jet-like flow located downstream of the step near the sidewalls and pointing towards the channel mid-plane, a thinner upper wall recirculation zone modifying the two-dimensional configuration of the flow, and a spanwise distribution of the primary reattachment line with a maximum reattachment length at the sidewall and a minimum reattachment length close to the wall (increasing then again when moving towards the mid-plane).

Rani et al. [19, 20] and Sheu and Rani [21] performed simulation of the flow behaviour on a geometry analogous to the one used by Armaly et al. [18] with AR = 8 and ER = 2, and at laminar and transitional regimes. The studies assessed the effect of sidewalls on the flow and the shed vortical structures downstream the BFS. A detailed description of the flow downstream of the BFS was obtained, and the three-dimensionality of the flow is associated with Kelvin-Helmholtz instabilities and Taylor-Gortler-like vortices.

Tylli et al. [22] and more recently Malamataris [23] present results of experimental and numerical simulations over a three-dimensional BFS with an AR = 40 and ER = 2 for laminar flow (low Re). The effect of lateral walls on the primary and upper wall recirculation zones was demonstrated. The studies relate the onset of unsteadiness with the presence of sidewalls and propose that the transition to three-dimensional flows is due to the growing penetration of the wall-jet from the sidewall to the central symmetry plane.

The studies on BFS geometry have been extended with the inclusion of the heat transfer through the chamber walls. When heat transfer is present, the mixing process of high and low

energy flows occurs in the reattachment region impacting significantly the mechanism of heat transfer and the flow behaviour.

Many works have been devoted to investigate heat transfer characteristics of BFS flow, on laminar and near the transitional regimes in two-dimensional [24, 25] and three-dimensional geometries [16, 26, 27, 28] and on turbulent regime [29].

Iwai et al. [26] investigate the effect of channel aspect ratio for a Reynolds number equal to 250 and including heat transfer through the bottom wall. They show contours of Nusselt number (Nu) and friction coefficient on the bottom wall and found the maximum Nu near the lateral wall and that the value of this maximum increases with the aspect ratio. Nie et al. [16] present results of numerical simulations for low Reynolds number (100-400) on a BFS with AR = 8. The peak in the Nusselt number increases with the step height and appears in the same region where the reattachment length is minimum. In the manuscript, the authors propose that the impingement of the wall-jet flow on the step wall is the cause. Xu et al. [28] investigate the fluid flow and heat transfer characteristics for a 3D backward facing step with aspect ratio 16 in the range of Re 200-1200. The authors use air as fluid, assuming constant properties, including density. For Re = 1000, they show K-H instabilities in the central plane of the channel. However, these results disagree with the study carried out by Xie [25] for a two-dimensional BFS, in which the vortex appear for a Re (based on the step height s) greater than 500, that is, a Re based on 2s greater than 1000. Also, several studies can be found in the literature on BFS with heat transfer enhancement by local forcing with suction and blowing or pulsating flow [30, 31 32]. Those studies are focused on two-dimensional geometries.

However, few studies have addressed backward-facing step flow on three-dimensional geometry in narrow channels, i.e., at aspect ratios smaller than 8, such as those found in actual geometries of internal flows systems used in heat transfer applications, such as turbine blade cooling channels with ribs, in which the effect of the sidewalls on the topology of the flow is more relevant. The previously cited work from Iwai et al. [26] investigate the thermal flow over BFS with AR = 4 for Re=250. Barbosa et al. [33] study the effect of Richardson number in a BFS flow with AR = 4 and for a single Reynolds number (Re = 200).

Due to this lack of studies in narrow channels, the authors [34] recently published a numerical and experimental study of the adiabatic ~~compressible~~ flow of a ideal gas over a BFS with aspect ratio ranging between 4 and 8 to provide deeper insight into the three-dimensionality occurring in the separated flow inside a narrow channel, focusing on the secondary recirculation bubble formed at the upper wall of the channel and its effect on the development of different three-dimensional flows, and the corresponding hydrodynamic action. The simulations were validated with experimental results obtained from flow visualization techniques.

To the authors' knowledge the thermo-convective airflow over a narrow BFS channel (with low aspect ratio) for the range of Reynolds number 100-1200 has not been investigated yet and this gap in the literature demonstrated in the foregoing review has motivated the present study. Therefore, the aim of the present work is to assess the effect of the side-walls on heat transfer features of the backward facing step in a narrow channel at laminar and early transitional regimes. The study is presented like natural extension of the studies performed by the authors [34] without heat transfer, and it is performed by means of Large Eddy Simulations using two different wall boundary conditions (slip and non-slip) to separate the wall induced phenomena from the inherent 3D flow structures.

The paper is organized as follows. Section 2 presents the description of the problem and the numerical model used in the study. Section 3 evaluates the accuracy of the mesh through a mesh independence analysis. The computational code used in the present work and the numerical model for adiabatic walls was already validated in the previous work, for this reason in Section 4, the effect of heat transfer is validated against data published for Re = 400 and AR = 8. The authors have developed an experiment to provide a qualitative insight of the flow behaviour. The experiment consists in the use of Moiré interferometry technique in the same investigated geometry. Section 5 discusses the results obtained from the simulations analysing the effect of sidewalls on heat transfer phenomena. Finally, Section 6 summarizes the main conclusions of the study.

2. Problem formulation and numerical model

The numerical procedure used in the present work is the extension of a previous study by the authors [34] to a heat transfer problem. The problem studied is the three-dimensional convective airflow in a rectangular channel with a backward facing step. The flow is modelled by time-dependent Navier-Stokes equations combined with an equation of state for the flow, which in the case of air is the ideal gas law, defined as follows:

$$\rho = \frac{p_{OP} + p}{R_g T} \qquad (1)$$

Where p is the predicted local relative pressure and p_{OP} the operating pressure. The range of flows studied includes laminar and early transitional flow regimes ($100 \leq Re \leq 1200$). The distinction between the different flow regimes is not obvious and depends on the flow configuration. In such flows, the unsteady Reynolds-averaged Navier-Stokes equations with advance high-order turbulence models for closure do not have enough precision because of underlying assumption that flows are fully turbulent. In addition, the empirical constants and functions of the Reynolds stress equation model are adjusted for a general case, but they must be modifies to match the condition of a particular flow field, and consequently the applicability of the model must be carefully examined.

For this reason, large eddy simulation (LES) was used in a previous study performed by the authors to describe the influence of side-walls and the structure of the flow in BFS with low aspect ratios. LES is a numerical approach to solve the flow behavior that lies between RANS and DNS, currently used for understanding the physics of flows where laminar and transitional regimes are present [35, 36], and for the description of complex mechanisms of heat transfer in forced-mixed convective flows [37].

LES formulation is based on the filtering of flow Navier-Stokes equations to separate large eddies from small ones. The large eddies are resolved on grid scales, whereas the smaller scales are modeled using a sub-grid scale (SGS) model. Consequently, the simulation requires fewer empirical modeling, thus obtaining a more accurate solution than URANS formulations.

The complete set of spatially filtered, Favre-averaged form of the governing equations of the conservation of mass, momentum and thermal energy for compressible flow in a Cartesian coordinate system can be seen in references [38, 39].

The sub-grid scale terms τ_{ij}^{SGS} and q_j^{SGS} can not be computed directly, and it is where the sub-grid scale (SGS) model is needed. One of the most used models is the Smagorinsky formulation for compressible flow [40]. In this model the SGS terms are given by

$$\tau_{ij}^{SGS} = C_s \Delta^2 \rho \left|\overline{S}\right| \overline{S}_{ij} \qquad (2)$$

$$q_j^{SGS} = C_s \Delta^2 \rho \left|\overline{S}\right| \frac{\partial \overline{T}}{\partial x_j}$$

where Δ is the low pass filter width calculated from local grid spacing, $\Delta = \left(\Delta_x \Delta_y \Delta_z\right)^{1/3}$, S_{ij} is the rate of strain tensor for the resolved scale defined as

$$\overline{S}_{ij} = \frac{1}{2}\left(\frac{\partial \overline{u}_i}{\partial x_j} + \frac{\partial \overline{u}_j}{\partial x_i}\right) \qquad (3)$$

and thus $\left|\overline{S}\right|$ the magnitude of the strain rate defined as

$$\left|\overline{S}\right| = \sqrt{2\overline{S}_{ij}\overline{S}_{ij}} \qquad (4)\ .$$

In Smagorinsky's formulation the coefficient Cs is fixed in advance and must be tuned to properly characterize transitional-laminar flow and near wall flow for the particular configuration under study. To obviate the need to specify the coefficient Cs in advance, Germano et al. [41] and Lilly [42] developed the dynamic Smagorinsky model, a procedure in which Cs is dynamically computed based on local flow conditions.

In the present work, the abovementioned Navier-Stokes governing equations have been solved using a large eddy simulations approach with the dynamic Smagorinsky subgrid scale model in a well-established computational fluid dynamic code, the commercial CFD package Ansys-Fluent. The code discretizes the governing equations on a non-uniform hexahedral mesh using a finite volume approach [43]. An implicit pressure based solver was used in conjunction with an algebraic multigrid method. For the transient formulation a non-iterative time advancement was followed with a typical time increment of 10^{-5} to ensure that the maximum CFL was lower than 0.5 for the higher Re studied. The pressure-velocity coupling was achieved using the PISO algorithm with neighbour correction and the spatial discretization with bounded central differencing scheme for momentum equations [43].

The dynamic Smagorinsky formulation in the code is based on work of Germano [41] and the procedure is executed using the development of Kim [44]. The dynamic stress and dynamic energy flux LES model options were selected for the analysis.

A sketch of the geometry corresponding to the computational domain with the nomenclature, main dimensions and coordinate system is depicted in Figure 1. The geometry of the duct with the backward facing step is similar to the one used by the authors [34], with an expansion ratio, ER=H/s =2 , where H is the height of exit channel and s the step size, and with an aspect ratio AR=W/s= 4, where W is the channel width.

Constant and uniform temperature and stream-wise velocity profiles are imposed as inlet conditions and a pressure outlet condition was applied as boundary condition at the exit plane (zero gauge pressure).

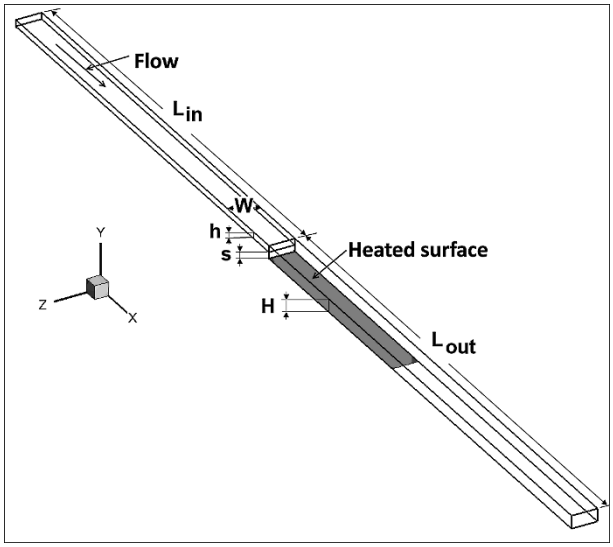

Figure 1.Sketch of the computational domain with the main dimensions indicated in the figure

The length of the channel upstream of the step used in the present work, L_{in}, is enough to ensure a developed velocity profile over y-axis until Re≈1200, according to the correlation provided by Durst et al. [45] for laminar flow in two-dimensional channels given by:

$$L_{in}/h = [(0.619)^{1.6} + (0.0567 \cdot \mathrm{Re})^{1.6}]^{1/1.6} \quad (5)$$

This correlation leads to a total inlet length, $L_{in}/s = 68.3$. Moreover, the non-dimensional velocity profiles at the step over the y-axis obtained numerically for all Reynolds studied in this work coincide, which ensures the proper flow development at the entrance. The definition of the Reynolds number used in the present study is the same one used by Armaly et al. [6], and it is based on the height of the step and the average inlet velocity, as:

$$\mathrm{Re} = \frac{\rho_0 u_0 2h}{\mu} \quad (6),$$

where ρ_0 is the density in the channel inlet, μ the viscosity of the air at the inlet temperature and h the inflow channel height, which is equal to the step size, s. The exit plane was located far enough from the step to minimize the effects of the outflow conditions on the results obtained in the zone of study near the step. The length behind the step, L_{out}, was selected in order to ensure that the boundary condition at the exit plane does not alter the results in the region near the step, as previously shown by Juste and Fajardo [34]. To confirm this assertion, in addition to the correlations of the bibliography and previous results, several numerical tests were performed for Reynolds number 1200. The results obtained confirm that in the range of Reynolds numbers studied, a longer domain does not modify the flow in the region of the step. Figure 2(top) presents the velocity profile for two different possitions and two domain lengths (Long domain: Lout/s=82 and Short domain: Lout/s=35) and Figure 2(bottom) show the corresponding temperature distribution. In both cases the curve seem to coincide. In any case, and to ensure the independence of the results with the domain length, in this work the cases with high Re numbers (Re>=1000) corresponding to early transitional flow, have been

computed using the longer domain to analyze the flow downstream of the primary recirculation bubble.

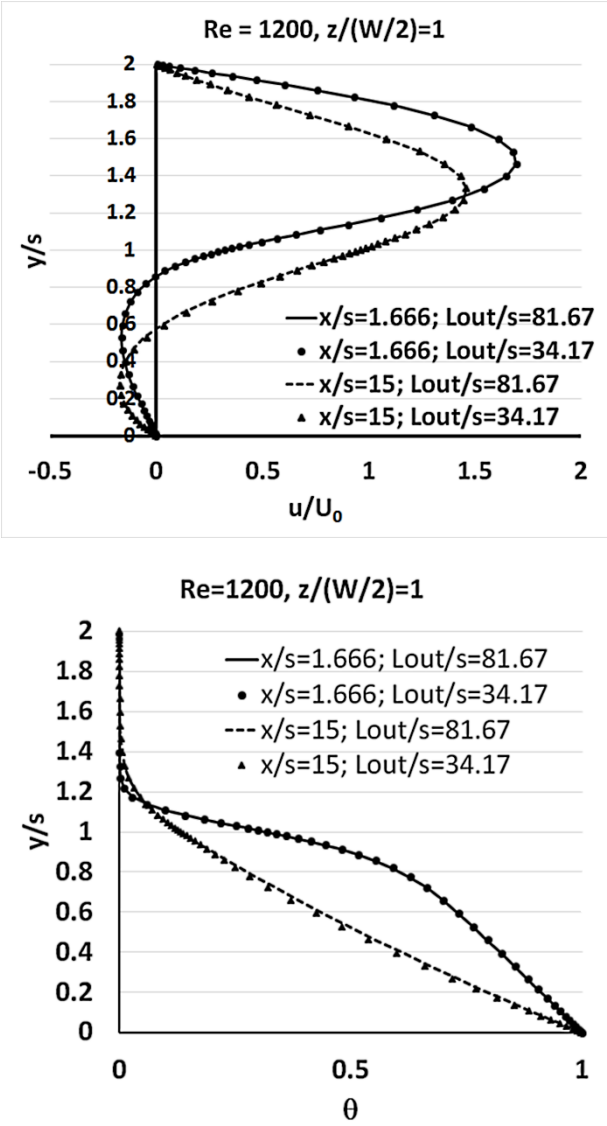

Figure 2. Comparison of the velocity profiles (top) and the temperature distribution (bottom) for the two domains used. The different in length does not seem to affect in the region of the step

Where θ is the non-dimensional temperature, defined as follows:

$$\theta = \frac{T - T_0}{T_{hot} - T_0} \qquad (7)$$

A non-slip wall condition was imposed at the top and bottom walls, and the step wall. However, with the aim of isolating the effect induced by the side-walls of intrinsic three-dimensional effects, two different boundary conditions were applied in the lateral walls, a non-slip wall condition, and afterwards, a slip wall.

During the calculations, the temperature of the heated surface (with a length L_{hot} = 34s) in the bottom wall is kept constant, and equal to a temperature T_{hot} greater than T_0, for all Reynolds numbers studied (Richardson number is smaller than 0.1 for all Reynols numbers above 300, and smaller than 0.01 for Re=1200, i.e. forced convective flow), while the rest of the walls

were considered adiabatic. The length of the heated surface is the same as that used in the experimental tests and it is greater than the reattachment length for all the Reynolds studied.

The convergence criteria were set such that RMS-residuals must be smaller than 10^{-5} for the mass, velocities and energy, and in addition, a statistically stationary state is reached. Data sampling for time statistics started after a few residence times in the domain, depending on the Reynolds number. This averaging time continues at least 200000 time steps. For cases with low Reynolds number (<1000), the solution was shown to be steady; for highest Re, the time averaging over the last 10000 time steps was used.

3. Grid-mesh dependence analysis

In a previous work by the authors [34], a grid-mesh independence study was conducted to ensure on the independence of the results of the cell size for the same computational geometry of the current work. Moreover, the solver and the computational procedure were validated for the case of adiabatic flow. In order to ensure the independence of the results in the case of forced convective flow with respect to the mesh size, an additional mesh-independence analysis has been made.

As a guideline, for a fully appropriate LES approach and to have confidence that the grid is capable of capturing an accurate well-resolved solution in the momentum and thermal boundary layers, the hexahedral mesh was designed with a near-wall distance y+<1. As a representative figure, for the final grid-mesh selected, the value of y+ in the Re=1200 case was 0.15 for the lower wall and 0.35 for the lateral and top walls.

The independence analysis was performed for the larger Reynolds number (Re=1200), and three mesh resolutions with fixed inflation and the same cell grow size ratio (1.2) were studied. The main characteristics of the three meshes compared in the study are summarized in Table 1.

Table 1. Main parameters of the three meshes compared in the independence analysis

Mesh	Cells	Initial element height (mm)	Maximum element size (mm)
M1	2164212	0.1	X: 0.65 Y: 0.25 Z: 0.5
M2	4082534	0.05	X: 0.65 Y: 0.2 Z: 0.35
M3	10297657	0.02	X: 0.45 Y: 0.15 Z: 0.3

Figure 3 shows a typical result obtained with the three meshes studied M1-M3, of the comparison of time-averaged velocity profiles in the direction of the flow stream in the mid-plane (Figure 3top) and in a plane near the side-wall (Figure 3bottom), for two streamwise locations (x/s) downstream from the step. In all cases, the profiles appear to overlap on a

single curve, especially those corresponding to the meshes M2 and M3. Additionally in Table 2 shows a fundamental characteristic of the problem, the reattachment length in the mid-plane. Increasing the mesh size by a factor greater than 2 ($4 \cdot 10^6 \rightarrow 1 \cdot 10^7$), results in a 0.26 % variation in the non-dimensional reattachment length.

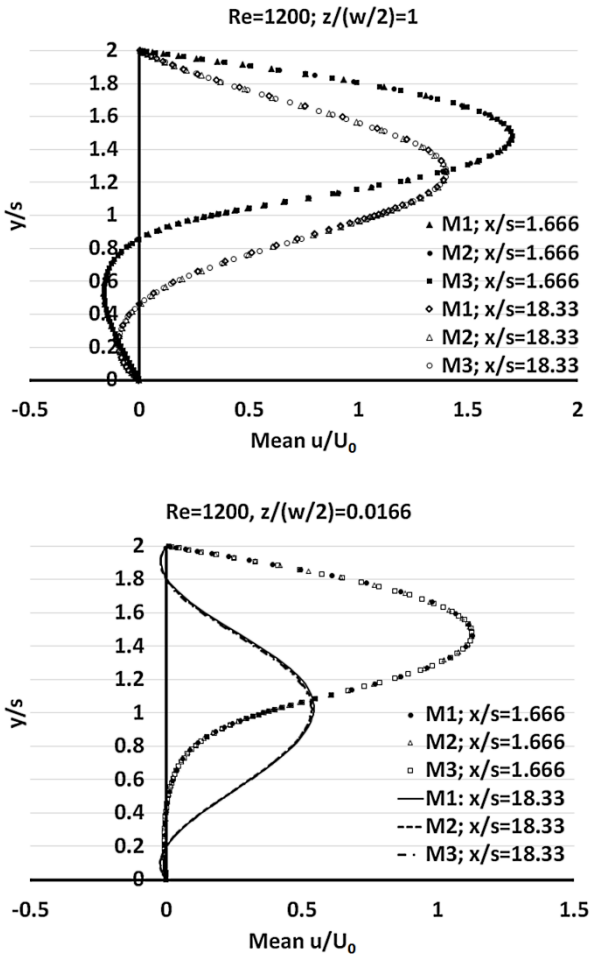

Figure 3. Comparison of the velocity profiles for the three meshes considered in the analysis for two different longitudinal coordinate and two spanwise positions: mid-plane (top) and close to the wall (bottom)

Table 2. Reattachment length obtained with the different meshes

Mesh	M1	M2	M3
Xu/s	25.583	25.766	25.833

The effect of the number of cells on the heat transfer is depicted in Figure 4, where the non-dimensional time-averaged temperature is drawn on the above-mentioned planes and locations corresponding to the velocity profiles.

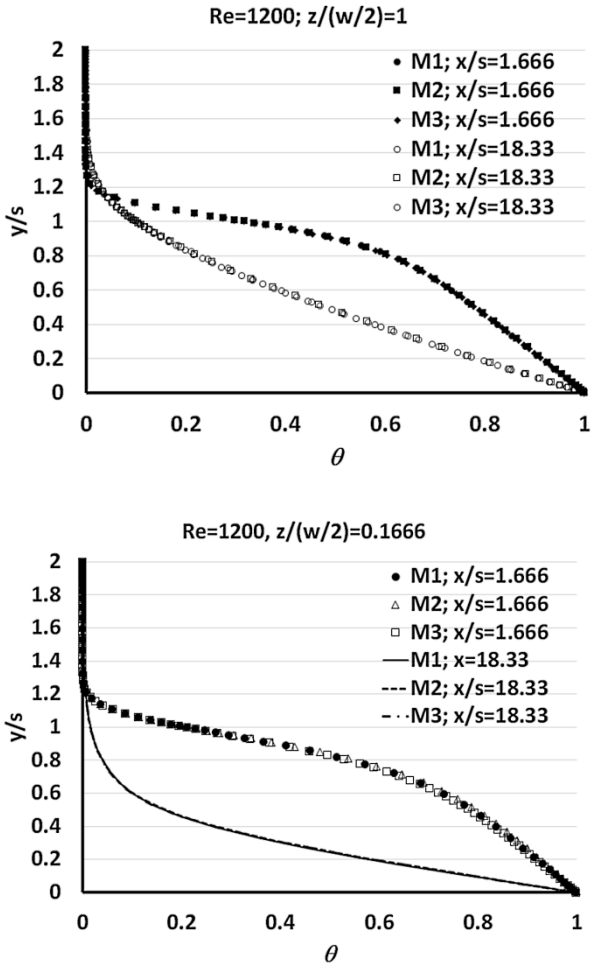

Figure 4. Comparison of the temperature distribution for the three meshes considered in the analysis for two different longitudinal coordinate and two spanwise positions: mid-plane (top) and close to the wall (bottom)

Figure 5 shows the time-averaged Nusselt number in the same xy-planes (constant z) as done before in the case of velocity profiles, the graphs appear to match, especially in the case of M2 and M3 meshes. To complete the mesh independence analysis, the same procedure followed in [34], based on the one described by Wang [46], was performed, obtaining similar results than in the previous work as shown in Table 3. In view of the above results, the differences between the meshes M2 and M3 do not justify the increase in computational cost of increasing the mesh size by a factor greater than 2, and therefore the mesh M2 was considered for the rest of the computational carried out in this work.

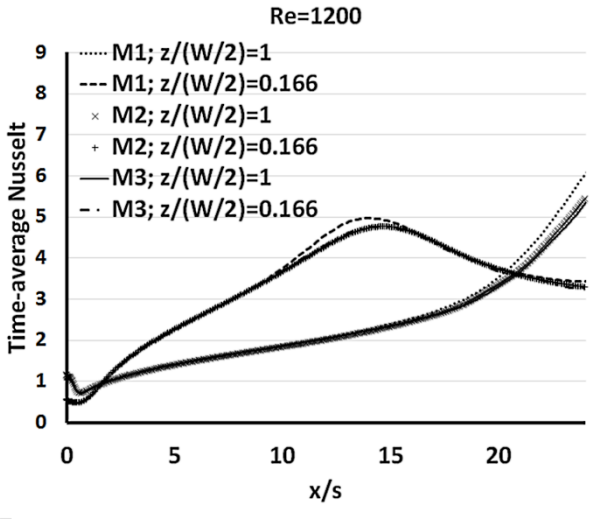

Figure 5.Time-averaged Nusselt number at the heated surface for the different meshes.

Table 3. Results of the mesh Independence analysis for Re = 1200.

Mesh	Cells	ε_1	E_2
M1	2164212	0.0124	0.0213
M2	4082534	0.00478	0.00455
M3	10297657	-	-

Based on these results, mesh M2 was considered for the rest of the computations performed in this work, in which the root-mean-square error in the velocity was less than 0.5%.

4. Model validation

The accuracy of the numerical model for the current geometry was validated quantitatively in the case of adiabatic flow in [34] against Armaly's experimental results [6] and by cross-comparing with the results obtained with another well-established code, FDS [47], and qualitatively against experimental results obtained by the authors in the case of adiabatic flow. A brief summary of the results for the case of adiabatic flow is shown in Figures 6, 7 and 8 where the numerical model was verified by direct comparison with the experimental results obtained by Armaly et al. [18] for a backward facing step with an aspect ratio equal to 8 for Reynolds number 343. Figure 6 and Fig. 7 show the non-dimensional velocity profiles in streamwise direction at different locations from the step (x/s=0 (Figure 6) and x/s= 1 and 7(Figure 7)). In general, the agreement is good, with slight discrepancies near the bottom wall in the case of x/s = 7. This discrepancies are probably due to uncertainty regarding the location of the measurement planes and digitization process of the data from the Figures presented in Armaly's paper.

The comparison of the numerical and experimental reattachment line computed according to the definition applied in Armaly et al. [18] is depicted in Figure 8. Again, the agreement was good across the channel width from the side-wall to the center of the duct.

4.1 **Quantitative validation of heat transfer model**

In addition to the previous results for the validation with experimental results in the case of adiabatic flow and, to gain confidence of the results obtained with the numerical model in the case of mixed-forced convective flow, a comparison with numerical results presented by Nie and Armaly [16] in a geometry with ER=2 and AR=8 for Re=400 has been carried out. In Nie's study all the walls were considered adiabatic, with the exception of the bottom wall downstream stepped wall that was treated as having a fixed and uniform heat flux q=50 W/m^2. As can be seen in Figure 9, where the Nusselt number along the z-axis at a streamwise location x/s=6.6 from the stepped wall is drawn, the agreement between both results is good, except in the central zone of the channel where slight differences are observed.

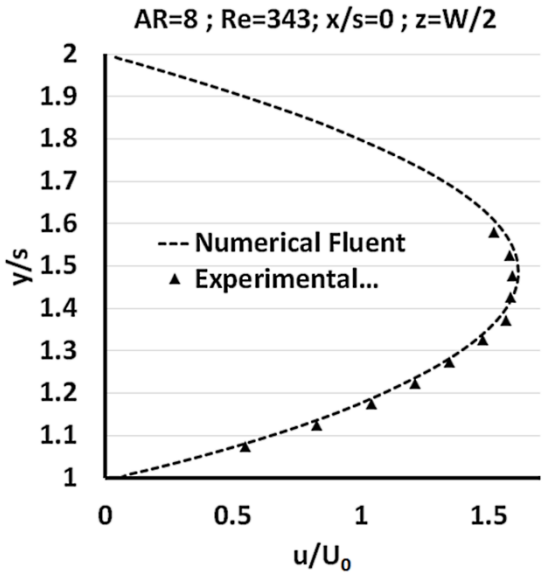

Figure 6. Comparison of the simulated velocity profile and the experimental results from Armaly at the step.

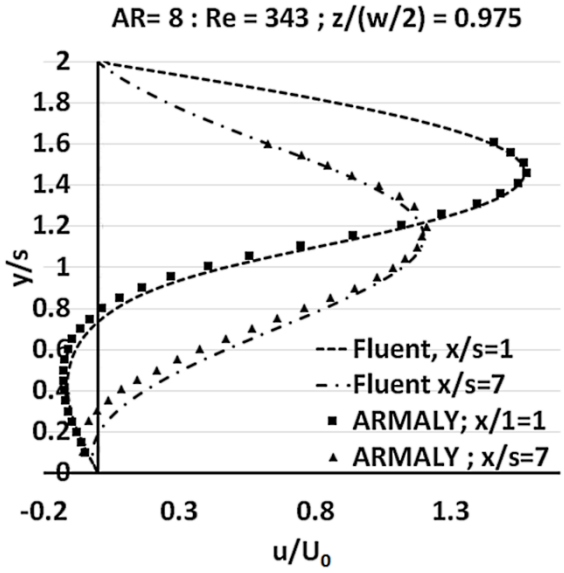

Figure 7. Comparison of the simulated velocity profile and the experimental results from Armaly downstream from the step.

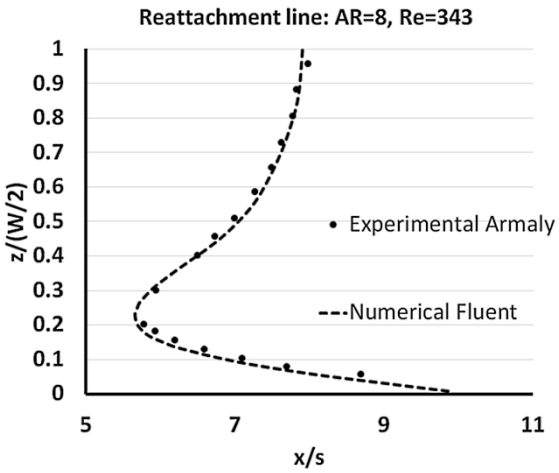

Figure 8. Comparison of the reattachment line simulated and obtained from the experimental results from Armaly.

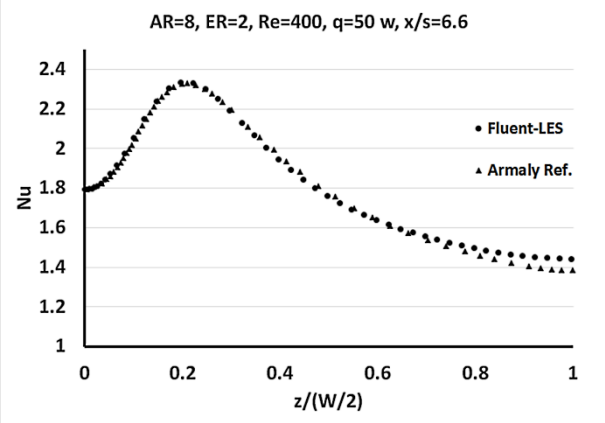

Figure 9. Comparison of the Nusselt at the heated surface number simulated and obtained from the experimental results from Armaly.

4.2 Experimental technique and comparison with numerical results

There are few experimental data of the thermal problem over the backward facing step in the literature to validate the numerical models, either quantitatively or qualitatively. Although most of the experimental works include detailed velocity measurements [6, 8, 48], wall shear rate measurements [49] and flow structure analysis (12, 22, 50]. The heat transfer is characterized only through pointwise measurement of the temperature with intrusive thermocouples probes [51] or recently, with infrared thermography on the bottom wall [52].

Juste and Benavides [53] performed an experimentally analysis of the local heat transfer over a BFS using Moiré deflectometry. This technique allows obtaining the temperature field downstream of the step wall, but the study was carried out on a BFS over a larger aspect ratio (AR=50) channel to assure the two-dimensionality of the flow, and for low Reynolds number (Re=162) and low temperature of the bottom wall, i.e. Richardson number, Ri, equal to 0.00385. Besides the heated surface behind the step was only ten times the step height.

The lack of experimental data on the temperature field behind of the step of BFS has led to the development of an experimental setup to obtain data useful to provide reliability of the

numerical model with heat transfer, at least from a qualitatively point of view, which together with the verification with data from the literature validates the numerical model. To do so Moiré deflectometry has been used in the present work to obtain experimental results for comparison purposes in the case study. The fundamental principles of Moiré deflectometry are presented in detail in Kafri et al. [54]. Moiré deflectometry, just like other optical techniques, is a line-of sight method and therefore it integrates the refractive index gradient throughout the path of transmitted light, then the results obtained are line-averaged values. This way the measurement of the refractive index gradient and the distribution of the related density gradient is straightforward only in two-dimensional flow or in the case of axisymmetric flow, by means of the Abel transform. Therefore, one of the limitations of the Moiré technique applied to three-dimensional flows is that it provides only beam-averaged fluid temperatures over the width of the channel.

Several published works present interferometric beam-averaged temperature and heat transfer data in a three-dimensional flow field. Naylor and Machin [55], carried out a beam-averaged temperature measurement in a three-dimensional temperature field using a two-dimensional analysis, but the experimental results did not agree with the defined bulk temperature. Sajith et al. [56] apply Mach-Zehnder interferometry to measure the heat flux in a three-dimensional channel (AR=1 and 2) with the bottom and top walls heated comparing the experimental results with theoretical results with measurements using thermocouples and obtaining a qualitative agreement with the thermocouple measurements. Juste and Benavides [57] applied Moiré deflectometry to external convective flow to study the end-wall errors in temperature measurement due to the edge effect only.

In the present study instead of obtaining a beam-averaged temperature, a two-dimensional phase map in the flow field will be obtained from experimental fringe pattern and then it will be compared with the phase map computed from the numerical results. Figure 10 shows a picture of experimental setup to obtain the temperature field in the backward facing step. A Phantom V311 camera is used to record the Moiré pattern displayed on a screen. This pattern is equivalent to that obtained by shearing interferometry with finite fringe alignment.

The sensitivity of the measurement is determined by the ratio δ/D, where δ is the pitch of the two gratings that are separated a distance D and tilted an angle α. To improve the sensitivity, the ratio δ/D should be reduced, but in this case the fringe pattern is blurred due to the diffraction caused by several factors, such as: poor beam quality, grating imperfection and inevitable diffraction due to the finite aperture of the optical system. These effects are discussed in detail in the works by Keren et al. [58] and Bar-Ziv et al. [59]. The gratings used for the present study were Ronchi Rulings with 10 lines/mm. The distance between the gratins and their pitch was selected to obtain suitable resolution and sensitivity, minimizing the above-mentioned diffraction effects. Moreover, the gap between the gratings was adjusted with a micrometer to an integer multiple of the distance known as the Talbot self-imaging plane to minimize the diffraction effects.

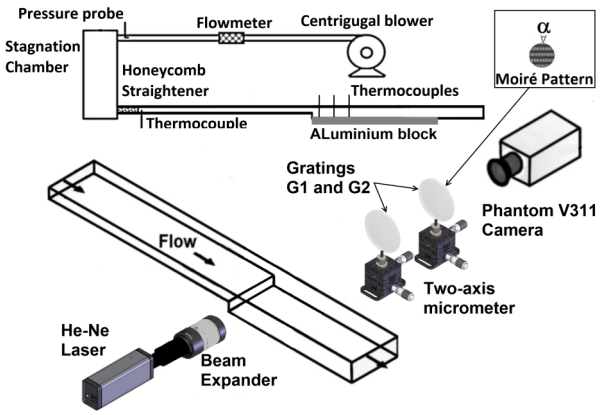

Figure 10. picture of experimental setup used in the present work

4.2.1 Evaluation of two-dimensional measurement

In this work, instead of evaluating the bulk-averaged temperature over the channel width from the two-dimensional Moiré pattern, that requires assuming a velocity profile over the z-axis; the phase change in the direction of flow (x axis) and in a perpendicular direction to the flow will be computed from the numerical data and compared with the experimental phase shift. Therefore, no additional hypothesis are needed.

The phase extraction method from the experimental fringe pattern is based on a two-dimensional Fast Fourier Transform (FFT). The detailed mathematical model is described in [60] and can be summarized in the following steps:

- Filter the images to remove noise and to select only the positive frequency components.
- Perform a frequency shift in the Fourier plane, so that the data are located around the origin.
- Apply the two-dimensional inverse Fourier transform.
- Determine the phase by evaluating the arctangent of the ratio of the imaginary and the real parts of the inverse transform.
- Unwrap the phase by adding multiples of 2π
- Remove any residual background phase

In the present work, the phase analysis based on FFT was carried out with the IDEA code [61]. The numerical results of the phase change are obtained with the following procedure:

- Three dimensional density field is obtained from the simulations.
- Gladstone-Dale law, is used to obtain the three-dimensional refractive index field, n(x,y,z) of the flow. The law stabilises: $n - 1 = K\rho$
- The refractive index gradient is computed in the direction perpendicular to flow direction (y axis), i.e., parallel to the fringes.
- Finally the phase shift in the test section is obtained
  $\varphi = \frac{2\pi D}{\delta}\frac{1}{n_\infty}\int_0^W \frac{\partial n}{\partial y} dz$

4.2.2 Description of experimental apparatus

The duct geometry and dimensions used in the experimental work corresponds to the geometry of the computational domain shown in Figure 1. A sketch of the experimental installation is shown in Figure 10. A centrifugal blower with an adjustable rotational speed, to regulate the mass flow, supplies the airflow to a stagnation chamber set upstream of a polycarbonate channel with a sudden expansion. The flow is passed across a honeycomb flow straightener before entering the duct to obtain flow uniformity at the channel inlet. The test section has two glass windows (instead of polycarbonate) to improve the flow visualization and to reduce errors caused by non-homogeneities in the polycarbonate and changes in the refraction index of the polycarbonate with the temperature. Lastly, the outlet of the channel is open to the free atmosphere.

The channel with the backward facing step is assembled to a micrometer-driven two-axis translation system, which enables aligning the area of the test section with the optical set-up and exploring the flow field downstream of the step.

The measurement of the mass flow with a hot-surface flow meter along with the pressure and temperature measurements at the channel inlet allows obtaining, applying the conservation of mass, an average velocity u_0, assumed to be uniform, which is used for the computation of Reynolds number.

The bottom wall behind of the step is composed of an aluminium block (L_{hot}/s= 34 and thermal conductivity = 180 $W \cdot K^{-1} \cdot m^{-1}$), which is heated by four heater mats feed with an adjustable DC power supply to maintain constant temperature for each Reynolds number. The heaters spans approximately the whole aluminum block, so the heating power is distributed as uniformly as possible over the block. Behind the heated surface, the bottom wall is made of polycarbonate up to the exit. Thermocouples type-K of 0.12 mm diameter wire are placed in the mid-plane on the surface of the bottom wall in different positions of the channel through the x-axis.

4.2.3 Uncertainty analysis.

In the experimental work developed in this work, two different types of meassures are considered: measures based on probes, and those based on optical methods. The estimation of uncertainty corresponding to the former ones is based on the method of propagation of uncertainties [62].

The error source in the calculation of the Reynolds number comes mainly from the measurement of mass flow rate ($\dot{m}$) through hot-surface flow meter. According to the sensor manufacturer's data, the Reynolds number has an estimated uncertainty of ±6%. The other source of uncertainty in the experimental results comes from the temperature measurement of the heated surface with thermocouples. In the problem studied the thermocouples are K type with special tolerance (±1ºC) and they are used inside a low radiative flux environment, therefore the error sources are constrained to conduction and velocity induced effects. Concerning the conduction effects, the thermocouples' junction exposed are set in contact with the heated plate, lead wires conduct heat away from the surface, thus altering the temperature to be measured. In the experimental setup and for the range of temperatures considered, the estimated uncertainty due to this effect is of the order of 2.5 ºC. Finaly, considering the velocity induced effect, assuming the insulated lead wire to be infinitely long, the heat loss can be modeled by fin type analysis. The estimated error is lower than or equal to 0.5 ºC. Therefore, considerint the combination of these effects, the uncerintanty on the heating surface temperature is roughly lower than a 4.5%.

Secondly, in the optical technique performed there are several sources of unceintanty. The first one of them is due to diffraction. The equation commonly used for the computation of the phase shift computation is:

$$\frac{\varphi}{2\pi} = \frac{\Delta\delta'}{\delta'} = \frac{D}{\delta}\frac{1}{n_\infty}\int_0^W \frac{\partial n}{\partial y}dz \quad (9),$$

where $\Delta\delta'$ is the displacement of Moiré fringes and δ' the spatial period of Moiré fringes. However as D increases to increase the sensitivity, this approximation falls, and due to diffraction, trace duplication appears. This effect produces an error in the estimation of the refractive index gradient [63]. For the grating period (δ)and the selected gap (D) used in the experiments to have adequate sensitivity, the error in the phase shift computation was approximately a 30%.

The other source of uncertainty was due to the heating of sidewalls and consequently the external convection and modification of temperature profiles inside the flow. A proper quantification of those errors is complex, and it would be requiere to measure with thermocouples the temperature distribution in the glass window (bot in the internal and external faces), and this measures would disturb the flow inside the channel.

4.2.4 Comparison with numerical results.

To compare with the numerical results, Moire deflectometry experimental technique was applied to the step geometry in the case Re = 500 and Richardson, Ri, equal to 0.05, where the natural convection is negligible and the flow velocity is not very low.

Before starting to record data from the Moire deflectogram, enough time was waited to ensure distribution of temperatures on the bottom wall as uniform and steady as possible. The measurements were started when no temperature variations were observed within the accuracy of the experimental equipment. Figure 11 shows a typical result of the temporal evolution of the temperature measurement with thermocouples in the experiments performed. As can be seen in the figure the differences between the thermocouples measurements are of the order of ±3.5%.

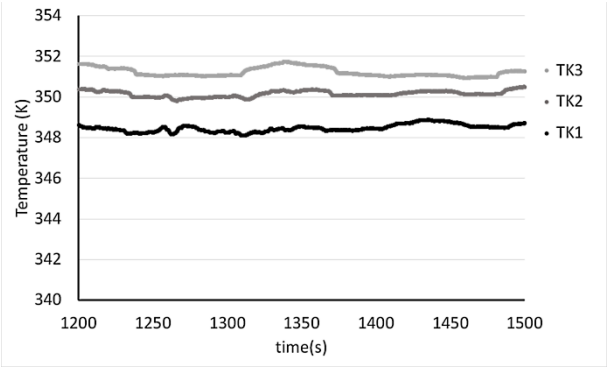

Figure 11. Temporal evolution of the temperature measurements with the three thermocouples, non-uniformities are of about 1.5%

Figure 12 shows a representative result of applying the two-dimensional fast Fourier transform (FFT) to a Moire deflectogram: figure 12(a) initial fringe pattern of the flow in the region of the step, Fig. 12(b) the module 2π phase map computed from the fringe pattern, and finally Fig. 12(c) presents the 2D phase field non-dimensionalized. The larger phase shift corresponds to the bottom wall downstream of the primary recirculation bubble and the shear layer formed after the step. The phase shift in Moire deflectometry represents the line-average of the refractive gradient along the width of the channel, therefore the maximum values of the gradient of the index of refraction occur in those zones. However, it should be noted that although the refraction index computed from the gradient may represent an average value, the corresponding temperature obtained does not represent the bulk temperature in the z-axis direction as previously mentioned, due to the three-dimensional flow originated by the side-walls in a narrow channel. On the other hand, since the waiting time necessary to achieve uniformity of temperatures in the heated bottom wall, is large, the temperature of the glass windows increases and thus varying the refraction index of the glass. This effect together with the natural convection in the external side glass windows should be taken into account when comparing it with the numerical results, especially in the case of backward facing step with low aspect ratios.

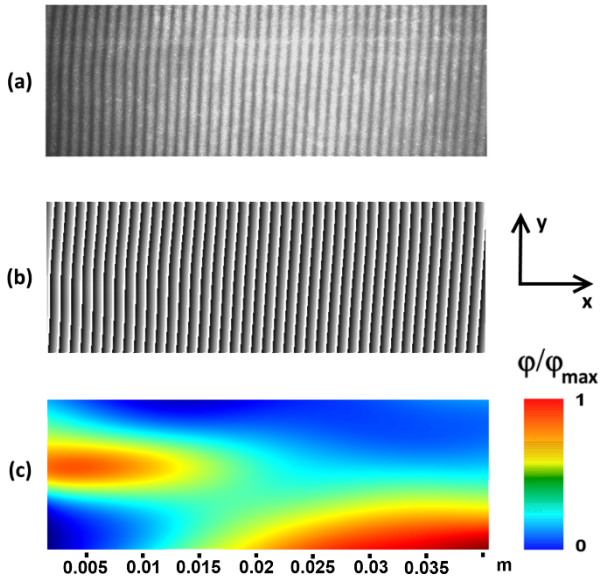

Figure 12. Moire deflectogram: (a) initial fringe pattern of the flow in the region of the step, (b) module 2π phase map computed from the fringe pattern, and (c) presents the 2D phase field non-dimensionalized

Correcting the phase shift map due to the heating of the sidewalls requires the computation of conduction effects in solids in the numerical model. For this reason, and for validation purposes only, the computation of thermal conduction through solid material of all channel walls coupled with the heat transfer in fluid (through the Conjugate Heat Transfer, CHT) was carried out. The thickness of the walls and the thermal conductivity of the solids used in the numerical computations was the same as in the experimental study. A sketch of the test section with the different materials used is shown in Figure 13. The grid resolution of fluid domain was the same one used in the rest of the work, that is, M2.

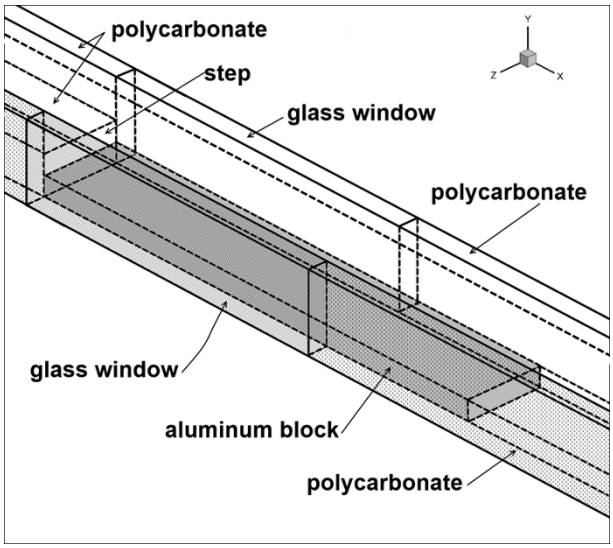

Figure 13. Sketch of the test section with the different materials used indicated.

Figure 14(top) shows several non-dimensional temperature contours at different streamwise locations in the case of conjugated heat transfer computations. These contours are obtained for a physical time of 100 seconds. Figure 14(bottom) shows the same contours in the case of adiabatic walls with exception of the bottom wall downstream of the step that is maintained at constant temperature. As observed when comparing the images, there are two effects: first, the temperature field is altered by the heat transfer through the the sidewalls. Second, the temperature is not uniform in the glass window. As mentioned in the uncertainty analysis, in order to make a quantitative comparison between the experimental and numerical results, it would be necessary to determine experimentally the temperature distribution inside and outside of the glass window, and to include in the simulation the natural external convection originated by this temperature.

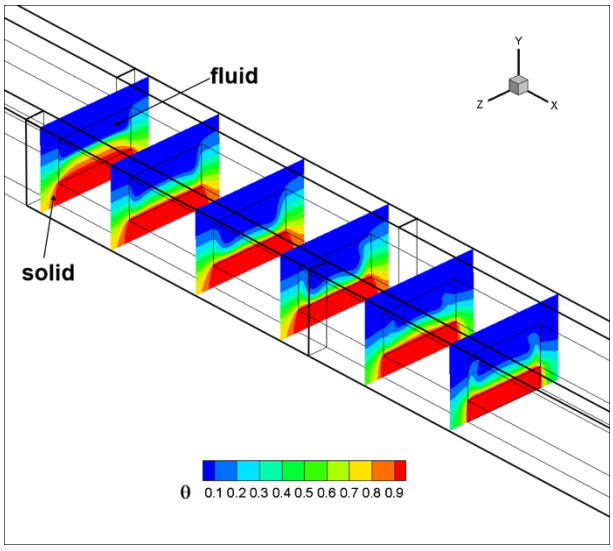

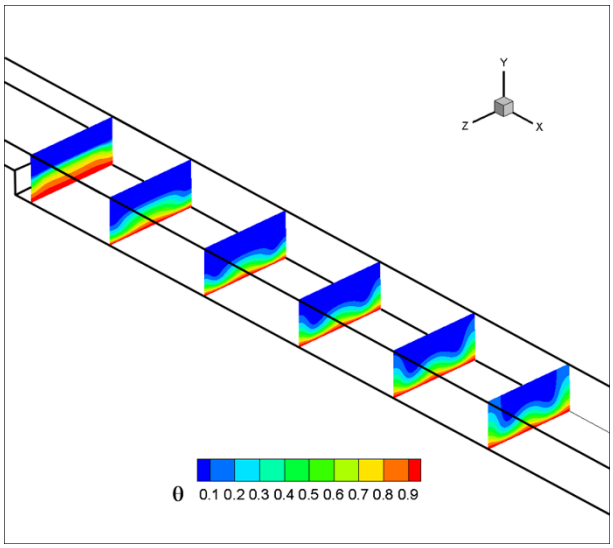

Figure 14. Comparison of the non-dimensional temperature contours of at different streamwise locations: (Top) for the computation including solid walls (CHT) and (bottom) with adiabatic walls.

However, as it can be seen in Figure 15 and Figure 16 where dimensionless phase shift contours on the test section and the dimensionless phase at a streamwise (x/s=1.66) location with the y-coordinate, are plotted respectively (φ_{max} is the maximum phase shift in the shear layer). The qualitative agreement between the experimental and numerical results is quite good, obtaining in both cases the maximum phase shift in the bottom wall and in the shear layer. The quantitative discrepancies are due, in addition to the previously mentioned effects, to quick changes of refractive index inside the flow along y-axis on a pitch scale (58), and the disturbance introduced by variations in the refractive index of the glass sidewall as its temperature increases.

The agreement found with published results and the qualitatively agreement with experimental results lends support to the validity of the numerical results obtained in the present work.

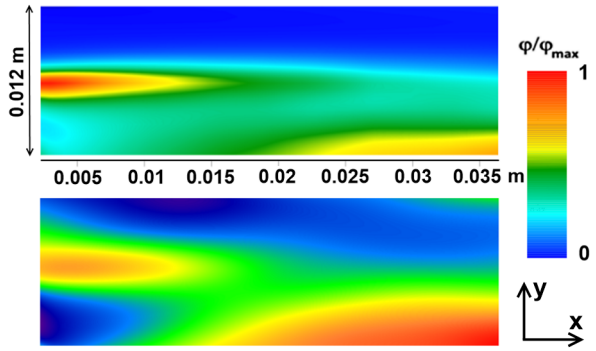

Figure 15. Comparison of the experimental (bottom) and numerical (top) dimensionless phase shift z-averaged contours.

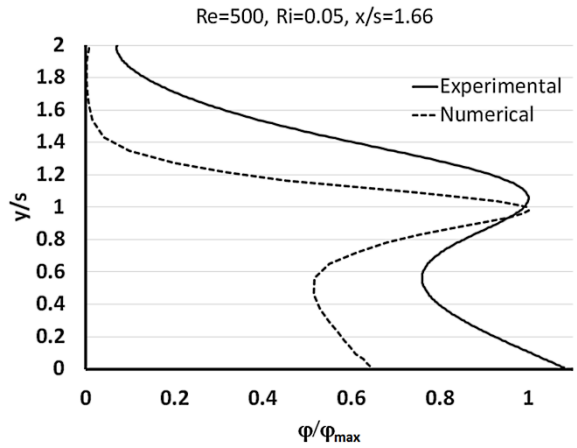

Figure 16. Evolution of the dimensionless phase with the y coordinate at a given streamwise section.

5. Results and Discussion

The objective of the present work is to assess the effect of the side-walls on heat transfer features of the backward facing step in narrow channels at laminar and early transitional regimes. With this objective, numerical simulations have been performed for AR= 4 and Reynolds number ranging between 100 and 1200 and keeping the heated surface just downstream of the step at constant temperature. The temperature selected provides a Richardson number between 10^{-3} and 1 for the range of Reynolds numbers investigated, i.e., forced-mixed convective flow.

The study covers the different aspects of three-dimensional flows induced by the presence of sidewall, i.e.: the wall-jet and the secondary recirculation bubble and its effect on the length of the primary recirculation bubble along the span, and comparing its effect on the characteristics of heat transfer with flows without sidewall effects and the effect of inherent three-dimensional flow features result of increasing the Reynolds number. The analysis is done through the simulation of the flow on the BFS with the same geometry but with two different boundary conditions at the walls: slip and non-slip walls.

The flow topology induced by the presence of lateral walls and its development by increasing the Reynolds in the case of mixed-forced convective flow are the same as for the adiabatic flow as in [34]. Figure 17(a) shows the wall-jets in a plane close to the bottom wall by plotting the streamtraces obtained forcing the streamtraces to remain in the slice plane for Reynolds 800. The figure includes the reattachment line, defined as the line at which the streamwise component of the velocity is zero. The flow going from the wall to the mid-plane, induced by the sidewall in the region of sudden expansion is increased by the upper wall recirculation zone adjacent to the lateral wall shown in Figure 17(b). These jets enhance the primary eddy at the mid-plane. Both the primary and secondary recirculation bubbles become larger as the Re increases, and the the upper bubble is moved downstream.

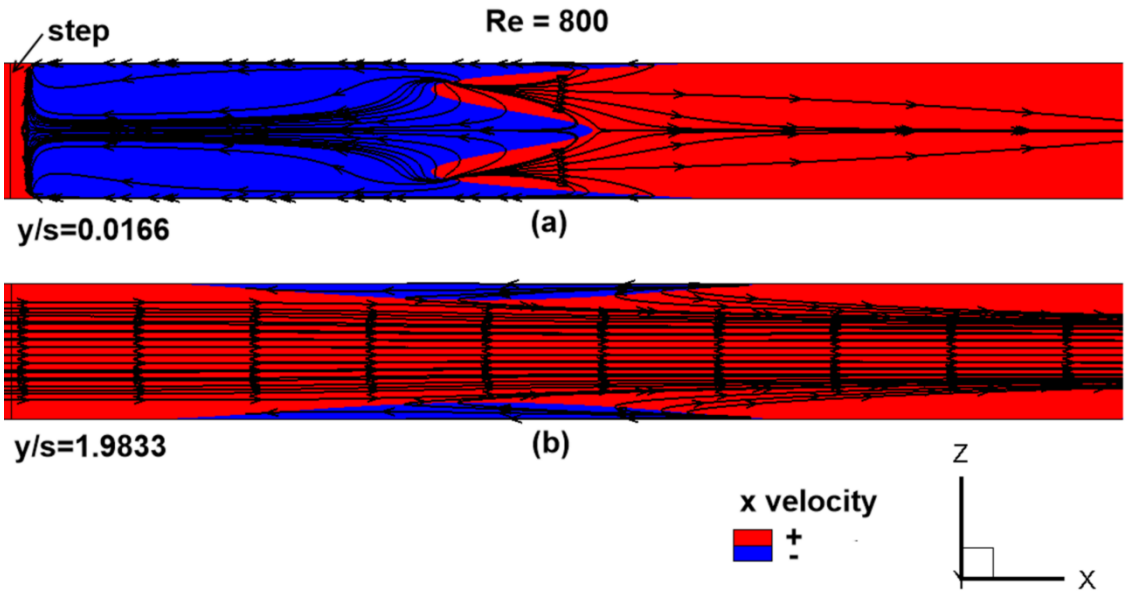

Figure 17. Contour of the sign of x-velocity component in a plane close to the bottom wall, the projection of the streamtraces on the plane are also plotted.

Figure 18 shows contours of streamwise velocity in two xy planes: one close to the sidewall (z=0.001) and another one at the middle plane (z=0.012). The three-dimensional streamlines are also presented. The streamlines show how the wall jets strengthen the primary bubble in the middle of the channel. The flow is symmetric and steady for low and moderate Re, lower than or equal to 1000, this means that the instantaneous and time-averaged values of velocities and temperatures are the same. Up to this Reynolds number, there are no three-dimensional flow feature other than those due exclusively to the effect of the sidewalls as shown in Figure 19, in which, velocity iso-contours, streamlines and vortex cores calculated with the λ^2 method described by Jeong and Hussain [64] for Re 800 and 1000 with free-slip boundary condition on lateral wall is depicted. For the same BFS three-dimensional geometry but enforcing a zero normal velocity and a zero normal gradient of streamwise velocity at the walls, the flow field is z-independent.

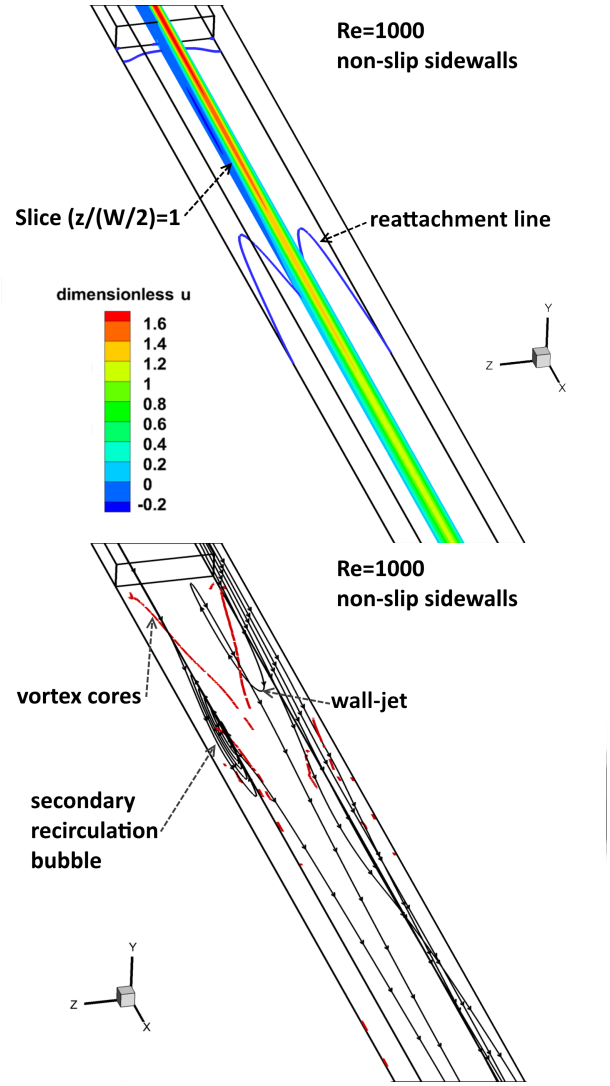

Figure 18. Contour of streamwise velocity at the middle plane (z=0.012) and reattachment line (a) and the 3D streamlines and vortex cores calculated with the λ^2 method (b).

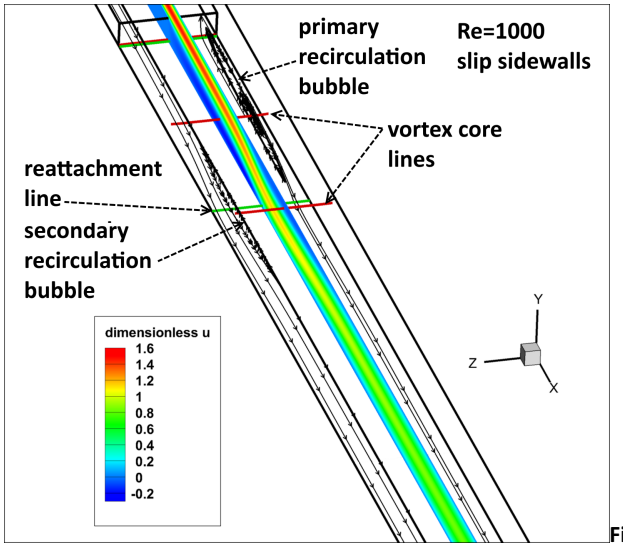

Figure 19. Velocity iso-contours, streamlines and vortex cores calculated with the λ^2 method for the case of slip walls. Flow two-dimensionality in this case is observed.

The reattachment line has the same shape than with no heat transfer, with a maximum length in the mid-plane due to the strengthening of the primary bubble by the wall jets and a minimum length at a spanwise position close to the sidewall due to the blockage effect of the upper recirculation zone adjacent to the lateral wall. This three-dimensional structure of the flow due to the effect of the sidewalls, which depends on the aspect ratio, becomes more remarkable as the Reynolds number increases as shown in Figure 20, where the reattachment line is drawn for the two boundary conditions applied on the lateral walls.

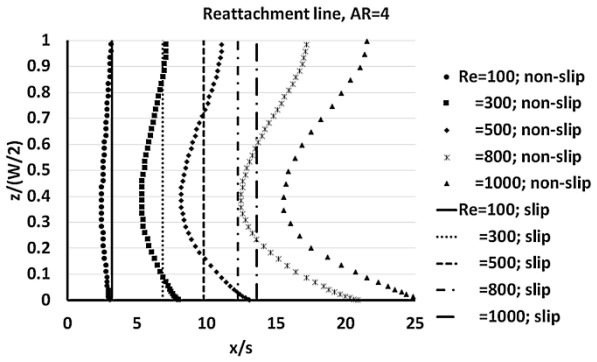

Figure 20. Velocity contours, streamlines and vortex cores calculated with the λ^2 method for the case of slip walls. Flow two-dimensionality in this case is observed.

At higher Reynolds numbers, the flow becomes unsteady and a three-dimensional structure appears. This structure is not caused by the three-dimensional geometry of the BFS (walls) with low aspect ratio but it is due to the turbulent flow behavior. These three-dimensional features are clearly evident for Re 1200, as shown in Fig. 21 where the flow characteristics for slip and non-slip boundary conditions on the sidewalls are compared. Figure 21a depicts the x-velocity at two planes, a xy plane located in the center of the channel and a horizontal plane near the bottom wall, besides the vortex cores lines, and in the figure 21b is drawn the stream-traces, both figures for the two boundary conditions. At Reynolds greater than 1000, the flow begins to show three-dimensionalities even when the slip boundary condition was enforced on the sidewalls.

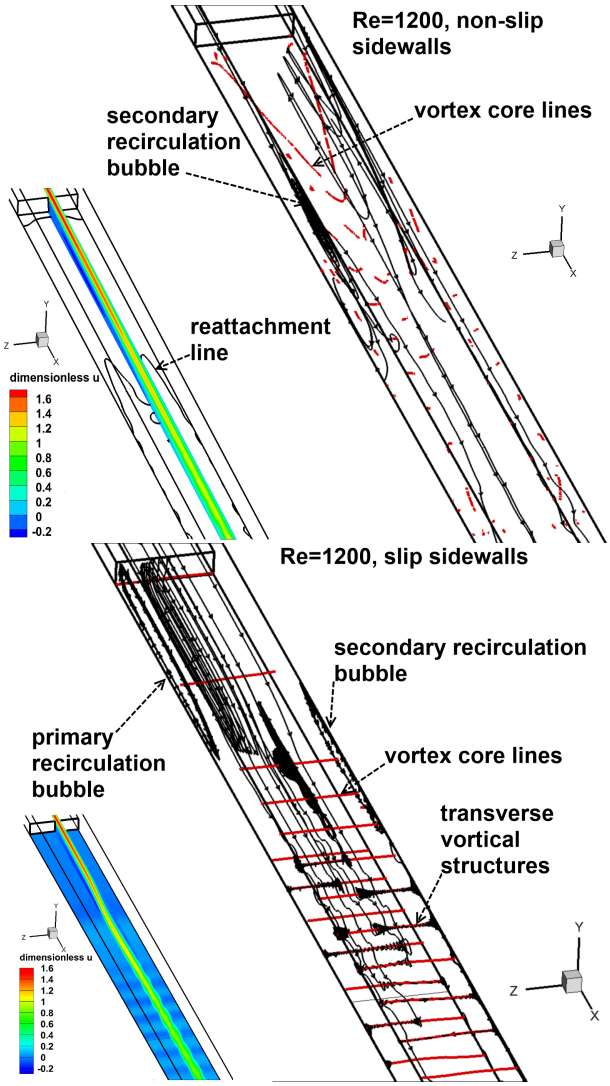

Figure 21. Velocity contours, streamlines and vortex cores calculated with the λ^2 method for the case of non-slip walls (a) and slip walls (b).

In the case of slip boundary condition, vortical structures appear along the top and bottom walls across the whole channel width. The streamtraces develop spirally around these vortex cores, thus inducing flow velocity in the z direction, which are not due to the lateral walls, but to intrinsic three-dimensional instability of the separated flow. However, in the BFS with non-slip sidewalls these vortical structures are not so evident because of the strong and dominant effect of the lateral walls on the flow through the wall jets.

This is evidenced using another method to identify the vortices, the so-called Q-criterion, in which coherent vortices are defined as space-time points with a positive second invariant of the velocity gradient tensor [65]. Figure 22 shows an isocontour of the normalized Q-criterion with slip and non-slip sidewalls from two different views: a xy-plane and a horizontal plane, both in the middle of the duct. Figure 23 presents a 3D perspective of the abovementioned structures. It is clearly perceived as in the case of slip sidewalls, the flow is no longer z-independent, whereas in the case of non-slip sidewalls the flow is nearly symmetrical. As mentioned above this is due to the strong effect that walls apply on the flow for settings with low aspect ratio, masking the intrinsic three-dimensional instability.

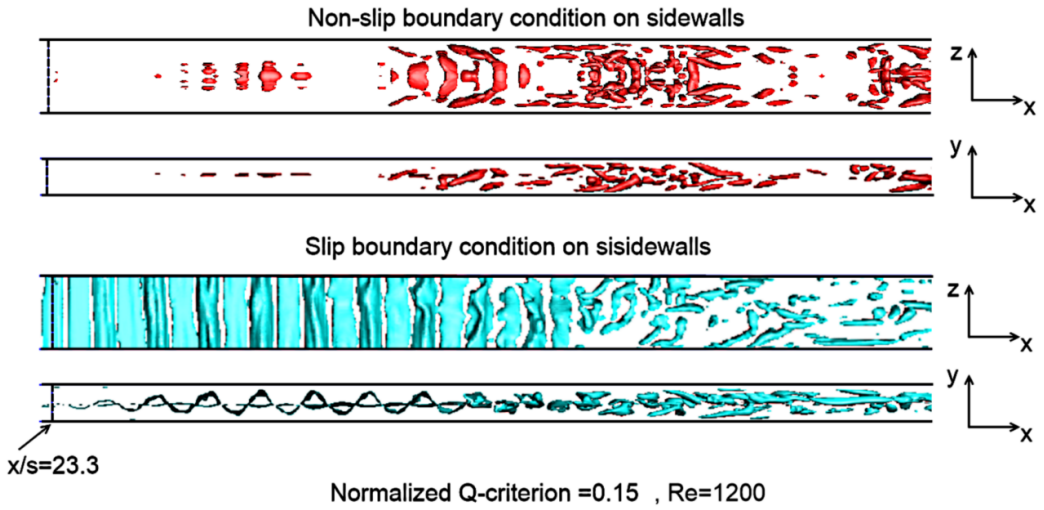

Figure 22. Iso-contours of Q-criterion (0.15) for the cases of slip and non-slip boundaries in the mid-plane of the channel.

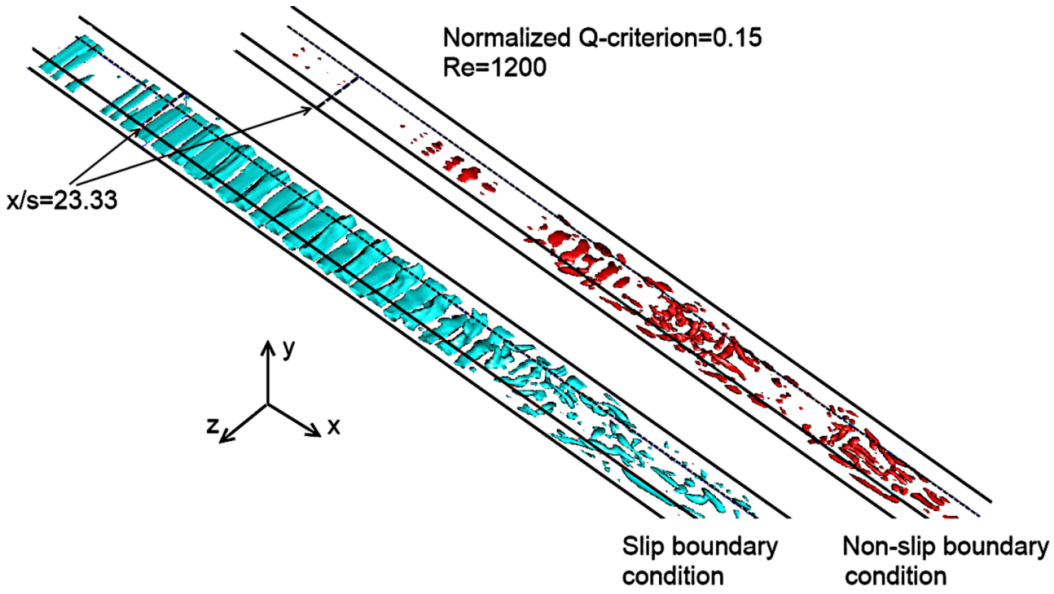

Figure 23. 3D view of the turbulent structures represented with the Q-criterion.

In addition, the three-dimensional instability that appears in the case of slip side-walls shows a periodicity with a fundamental frequency. Figure 24(top) shows the instantaneous velocity in the streamwise direction as a function of time and Figure 24(bottom) the FFT for the three velocity components at an arbitrarily chosen point in the flow field. However, in the case of non-slip sidewalls no fundamental frequency is clearly detected as can be seen in Figure 25. This intrinsic three-dimensional instability modifies the thermal boundary layer, increasing heat transfer as will be seen in the following.

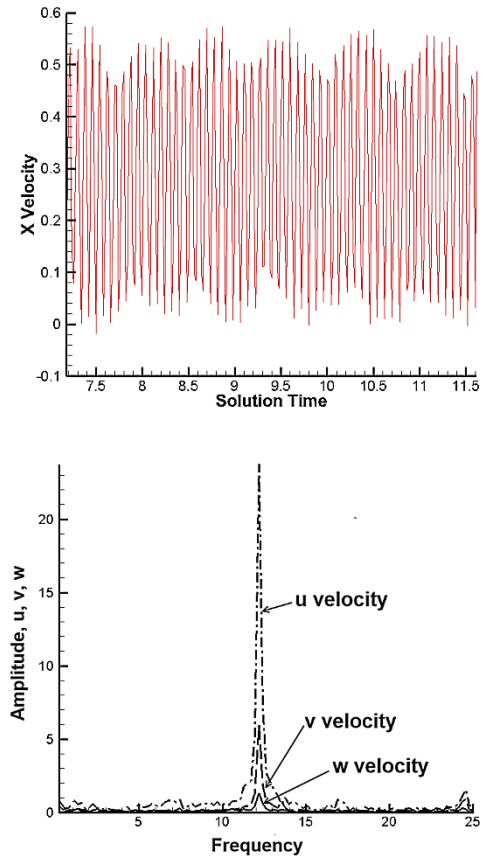

Figure 24. Top the instantaneous velocity in the streamwise direction as a function of time, and bottom the FFT for the three velocity components at an arbitrarily chosen point in the flow field. This is obtained for a case with a slip walls and a Reynolds of 1200.

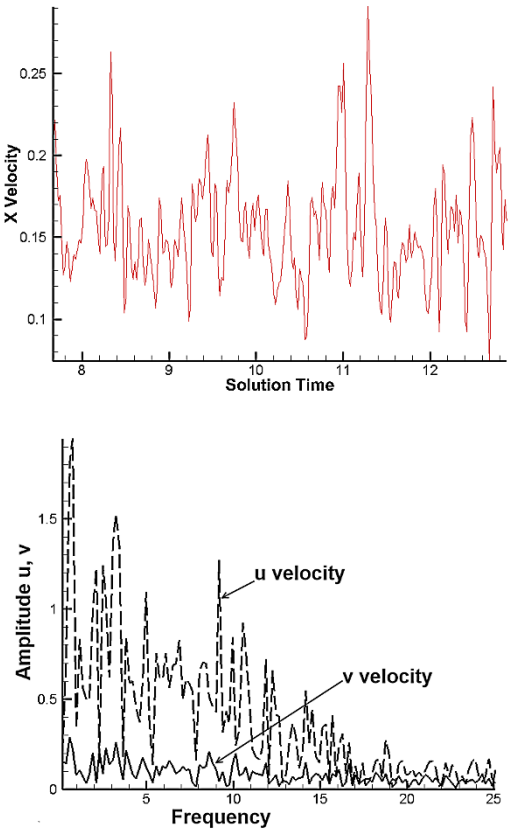

Figure 25. Top the instantaneous velocity in the streamwise direction as a function of time, and bottom the FFT for the three velocity components at an arbitrarily chosen point in the flow field for a case with a non-slip walls and a Reynolds of 1200.

The behavior of the Nusselt number over the hot plate in the case of non-slip sidewalls is similar for all Reynolds numbers studied, which for the selected plate temperature corresponds to mixed-forced convective flow. Figure 26 depicts the time-averaged Nusselt number isocontours on the heated lower plate, and the reattachment line and the streamtraces on a plane near the bottom wall (y/s=0.167) for Reynolds numbers 1000 and 1200.

The maximum of the Nusselt appears symmetrically near the sidewalls and in the same zone where the reattachment length is minimum. This coincides with the impingement region on the stepped wall and consequently, it seems to be associated the presence of wall jets coming from the lateral walls. Moreover, the zone of largest Nusselt numbers in the bottom wall of the channel is located in the wake downstream of this region. Increasing the Reynolds number, moves this maximum downstream as the reattachment line also does.

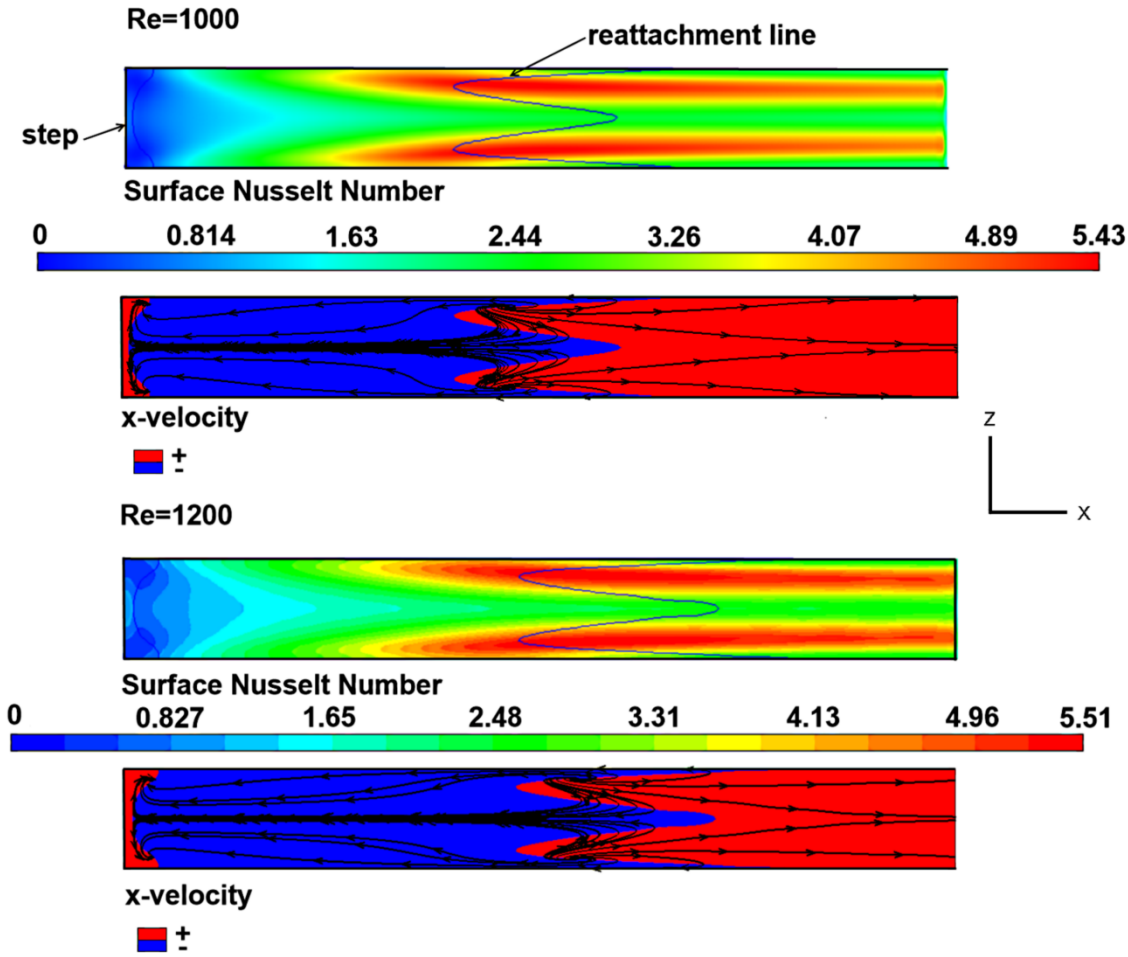

Figure 26. Time-averaged Nusselt number isocontours on the heated lower plate, and the reattachment line and the streamtraces on a plane near the bottom wall (y/s=0.167) for Reynolds numbers 1000 and 1200 and non-slip walls.

However, as shown in Figure 27, when the numerical simulation is performed with slip sidewalls, the Nu distribution on the heated plate is z-independent for Reynolds equal to 1000 with the maximum Nu appearing near of the reattachment line. For Reynolds 1200 the Nu distribution depends on z, and zones of high Nusselt numbers downstream of the primary recirculation zone appear. These zones coincide with the vortical structures on the bottom wall. Moreover, values of the maximum Nu in both cases are larger than those corresponding to the simulation with non-slip sidewalls.

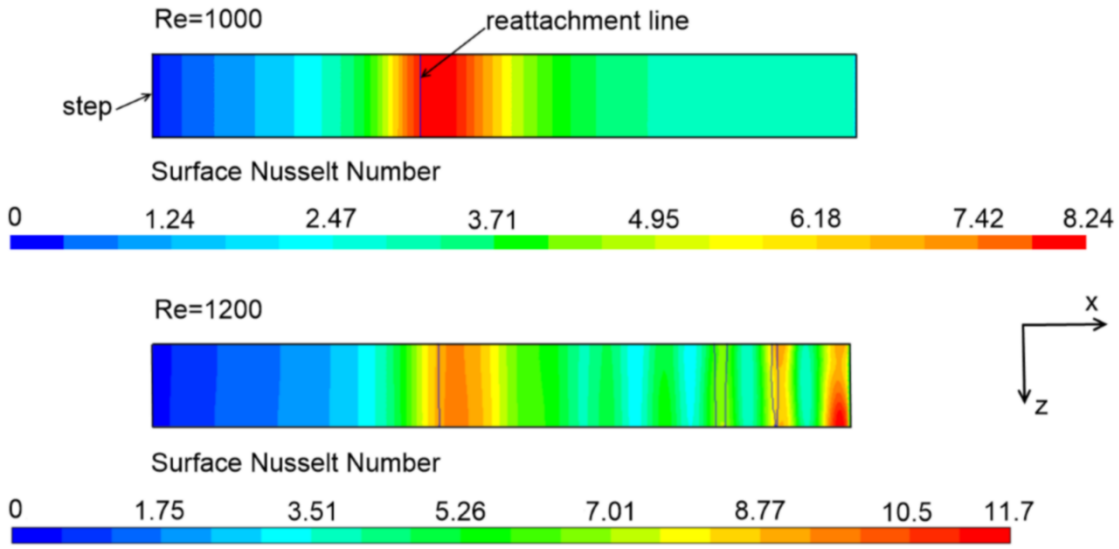

Figure 27. Time-averaged Nusselt number isocontours on the heated lower plate for Reynolds numbers 1000 and 1200 and slip walls.

This result is illustrated in more detail in Figure 28, where the spanwise average Nussselt number is plotted along the x-axis for Re 800, 1000 and 1200 for the two boundary conditions on lateral walls. The peak of Nu due to the primary recirculation bubble is significantly greater in the case of slip sidewalls for the three Reynolds. The Nusselt then decreases downstream, being lower than the corresponding values of the case with non-slip sidewalls. This is different in the Re 1200 case, where vortices across the width of the channel appear on the bottom wall downstream of the primary recirculation zone, yielding successive peaks of Nusselt number.

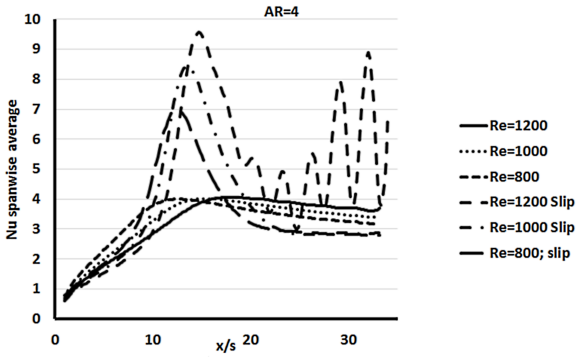

Figure 28. Spanwise-averaged Nusselt number evolution along the channel for different Reynolds and the two boundary conditions considered.

These findings are summarized in Figure 29, which shows the surface-averaged value of the Nusselt on the hot plate. For small Re, the Nu is larger with non-slip sidewalls up to Re 500. Then there is a change being greater the Nu with slip sidewalls. This effect is due in part to the movement downstream of the reattachment line by the increase of Re and the finite length of the hot bottom surface.

However, when intrinsic three-dimensional instabilities appear at Re 1200 there is a sudden change in the slope of the curve corresponding to the results with slip sidewalls. These instabilities are likely to be the cause of the heat transfer enhancement on the bottom wall,

which does not occur in the case of non-slip sidewalls where the wall jets that penetrate to the mid-plane damp the effect of the instabilities in BFS with low aspect ratio.

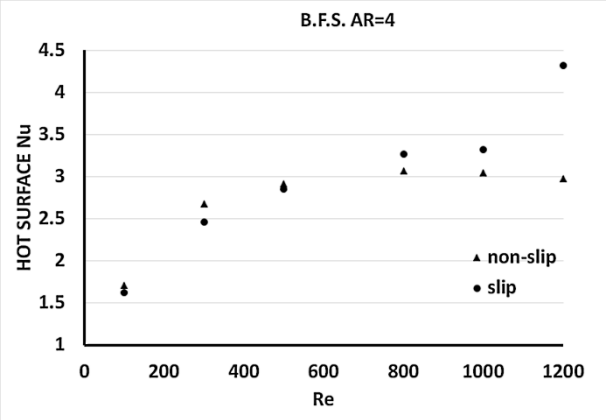

Figure 29. Surface-averaged Nusselt number evolution with the flow Reynolds number for the two boundary conditions considered.

6. Conclusions

This manuscript analyzes the effects of sidewalls on heat transfer phenomena in the flow on a narrow channel backward facing step geometry. The study is performed for laminar and early transitional regime as a function of Reynolds number. Large-Eddy Numerical Simulations were performed using the dynamic Smagorinsky formulation.

The results obtained show good quantitative agreement with experimental and numerical data from the literature used for verification and qualitatively with the experimental data obtained by the authors with Moiré deflectometry, in spite of the heat transfer in the lateral walls glass of the experimental setup, and the natural convection on the exterior of the lateral walls of the tunnel and diffraction effects, which alter the experimental measurements obtained.

To distinguish the three-dimensionality of the flow due to the effect of the lateral walls in ducts with low aspect ratio from the intrinsic three-dimensional instability of the turbulent separated flow, numerical simulations were performed with two boundary conditions on the sidewalls: slip and non-slip.

The numerical simulations show that for forced-mixed convective flow, the flow topology induced by the sidewalls, i.e. the outline and location of the reattachment line, wall jets and upper wall secondary recirculation zone, are the equivalent to those corresponding to the adiabatic flow.

When the heat transfer phenomena in the bottom wall downstream of the step is analyzed, it is observed that the maximum value of the Nu number appears in the zone where the reattachment length is minimum, near the lateral walls, even for the case for Re = 1200. However, when the slip boundary condition is imposed on the sidewalls of the BFS, the variation of the Nu on the heated lower surface is z-independent (i.e. two-dimensional flow) and the maximum value occurs in the reattachment zone, for Re smaller or equal than 1000. At the highest Reynolds (Re = 1200), when the intrinsic three-dimensional instabilities appear, the flow features depend on z and the value of the spanwise-averaged Nu is greater than that obtained with non-slip sidewalls.

This finding shows that the effects induced by the lateral walls in the case of BFS with low aspect ratio (AR=4) is so strong that it dampens the incipient effect of the three-dimensional instability that appears at the beginning of the transitional flow. As a result, the surface averaged Nu is greater in the case of slipwalls than in the case of non-slip sidewalls.

References

[1] J.C. Han, Recent studies in turbine blade cooling, International Journal of Rotating Machinery, 10(6) (2004) 443–457.

[2] S. Alfarawi, S.A. Abdel-Moneim, A. Bodalal, Experimental investigations of heat transfer enhancement from rectangular duct roughened by hybrid ribs, International Journal of Thermal Sciences 118 (2017) 123-138.

[3] J. Bucher, R.G. Edmonds, R.C. Steele, D.W. Kendrick, B.C. Chenevert, and P.C. Malte, The development of a lean-premixed trapped vortex combustor, ASME Paper GT2003-38236 (2003) 207-213.

[4] P.K. Ezhil Kumar & Debi Prasad Mishra, Numerical study of reacting flow characteristics of a 2D twin cavity trapped vortex combustor, Combustion Theory and Modelling 21(4) (2017) 658-676.

[5] J.K. Eaton and J. P. Johnston, A review of research on subsonic turbulent flow reattachment, AIAA J. 19(9) (1981) 1093‑1100.

[6] B.F. Armaly, F. Durst, J. C. F. Pereira, and B. Schónung, Experimental and theoretical investigation of backward-facing step flow, J. Fluid Mech. 127 (1983) 473-496.

[7] M.V. Otiigen, G. Papadopoulos, G. Vradis, and G. Muckenthaler, Spanwise Characteristics of the Separated Flow in a Suddenly Expanding Duct, Experiments in fluids 14 (1992) 213-216.

[8] T. Lee and D. Mateescu, Experimental and numerical investigation of 2-D backward-facing step flow, J. Fluids Struct. 12(6) (1998) 703‑716.

[9] L. Kaiktsis , G.E. Karniadakis and S.A. Orszag, Onset of three-dimensionality, equilibria, and early transition in flow over a backward-facing step, Journal of Fluid Mechanics 231(1991) 501- 528.

[10] L. Kaiktsis, G.E. Karniadakis, and S.A. Orszag, Unsteadiness and convective instabilities in two-dimensional flow over a backward-facing step, J. Fluid Mech. 321 (1996) 157‑187.

[11] D. Barkley, M.G.M. Gomes, and R.D. Henderson, Three-dimensional instability in flow over a backward-facing step, J. Fluid Mech. 473 (2002) 167‑190.

[12] J.F. Beaudoin, O. Cadot, J.L. Aider, J.E. Wesfreid, Three-dimensional stationary flow over a backward-facing step, European Journal of Mechanics B/Fluids 23 (2004) 147–155.

[13] P.T. Williams and A.J. Baker, Numerical simulations of laminar flow over a three-dimensional backward-facing step, Int. J. Numer. Methods Fluids 24 (1997) 1159-1183.

[14] T.P. Chiang and T.W. Sheu, A numerical revisit of backward-facing step flow problem," Phys. Fluids 11(4) (1999) 862‑874.

[15] G. Biswas, M. Breuer, and F. Durst, Backward-facing step flows for various expansion ratios at low and moderate Reynolds numbers, J. Fluids Eng. 126(3) (2004) 362–374.

[16] J.H. Nie and B.F. Armaly, Reattachment of three-dimensional flow adjacent to backward-facing step, J. Heat Transfer 125(3) (2003) 422–428.

[17] J. H. Nie and B. F. Armaly, Reverse flow regions in three-dimensional backward-facing step flow, Int. J. Heat Mass Transfer 47(22) (2004) 4713–4720.

[18] B.F. Armaly, A. Li, J.H. Nie, Measurements in three-dimensional laminar separated flow, International Journal of Heat and Mass Transfer 46 (2003) 3573–3582.

[19] H.P. Rani and T.W. Sheu, Nonlinear dynamics in a backward-facing step flow, Phys. Fluids 18(8) (2006), 084101.

[20] H.P. Rani, T.W. Sheu, and E.S. Tsai, Eddy structures in a transitional backward-facing step flow, J. Fluid Mech. 588 (2007) 43–58.

[21] T. W. Sheu and H.P. Rani, Exploration of vortex dynamics for transitional flows in a three-dimensional backward-facing step channel, J. Fluid Mech. 550 (2006) 61–83.

[22] N. Tylli, L. Kaiktsis, and B. Ineichen, Sidewall effects in flow over a backward-facing step: Experiments and numerical simulations, Phys. Fluids 14(11) (2002) 3835–3845.

[23] N. A. Malamataris, A numerical investigation of wall effects in three-dimensional, laminar flow over a backward facing step with a constant aspect and expansion ratio, Int. J. Numer. Methods Fluids 71(9) (2013) 1073–1102.

[24] T. Kondoh, Y. Nagano, T. Tsuji, Computational study of laminar heat transfer downstream of a backward-facing step, International Journal of Heat and Mass Transfer, 36(3) (1993) 577-591.

[25] W.A. Xie, G.N. Xi, M.B. Zhong, Effect of the vortical structure on heat transfer in the transitional flow over a backward-facing step, International Journal of Refrigeration 74 (2017) 465-474

[26] H. Iwai, K. Nakabe, K. Suzuki, Flow and heat transfer characteristics of backward-facing step laminar flow in a rectangular duct, International Journal of Heat and Mass Transfer 43 (2000) 457-471.

[27] G. L. Juste and P. Fajardo, Assessment of experimental optical techniques for characterizing heat transfer using numerical simulations, Eng. Appl. Comput. Fluid Mech. 9(1) (2015) 84–98.

[28] J.H. Xu, S. Zou, K. Inaoka, G.N. Xi. Effect of Reynolds number on flow and heat transfer in incompressible forced convection over a 3D backward-facing step. International Journal of Refrigeration 79 (2017) 164-175.

[29] H. Lan, B.F. Armaly, J.A. Drallmeier, Three-dimensional simulation of turbulent forced convection in a duct with backward-facing step, International Journal of Heat and Mass Transfer 52 (2009) 1690–1700.

[30] K. Khanafer, B. Al-azmi, A. Al-shammari, I. Pop, Mixed convection analysis of laminar pulsating flow and heat transfer over a backward-facing step, Int. J. Heat Mass Transf. 51 (2008) 5785–5793.

[31] S.R. Batenki and V.I. Terekhov, Friction and heat transfer in a laminar separated flow behind a rectangular step with porous injection or suction, Journal of Applied Mechanics and Technical Physics, 47(1) (2006) 12-21

[32] E. Abu-Nada, A. Al-Sarkhi, B. Akash, I. Al-Hinti, Heat transfer and fluid flow characteristics of separated flows encountered in a backward-facing step under the effect of suction and blowing, Journal of Heat Transfer 129 (2007) 1517-1528

[33] J. G. Barbosa Saldana, N. K. Anand, V. Sarin, Numerical simulation of mixed convective flow over a three-dimensional horizontal backward facing step, Journal of Heat Transfer 127 (2005) 1027-1036.

[34] G. L. Juste, P. Fajardo, and A. Guijarro, Assessment of secondary bubble formation on a backward-facing step geometry, Physics of Fluids 28 (2016) 074106.

[35] J. H. Ferziger and M. Peric, Computational methods for fluid dynamics, Springer Science & Business Media, (2012).

[36] M. Lesieur, O. Metais, and P. Comte, Large-eddy simulations of turbulence , Cambridge University Press, (2005).

[37] S. Kuhn, S. Kenjeres, P. Rudolf von Rohr, Large eddy simulations of wall heat transfer and coherent structures in mixed convection over a wavy wall, International Journal of Thermal Sciences 49 (2010) 1209-1226.

[38] E. Garnier, N. Adams and P. Sagaut, Large eddy simulation for compressible flows, Scientific Computation, ISBN 978-90-481-2818-1 Springer (2009).

[39] Favre averaged Navier-Stokes equations, https://www.cfd-online.com/Wiki/Favre_ averaged_Navier-Stokes_equations (2017)

[40] J. Smagorinsky, General circulation experiments with the primitive equations. I. The basic experiment, Mon. Weather Rev. 91(3) (1963) 99‐164.

[41] M. Germano, U. Piomelli, P. Moin, and W. H. Cabot, A dynamic subgrid-scale eddy viscosity model," Phys. Fluids A 3(7) (1991) 1760‐1765.

[42] D.K. Lilly, A proposed modification of the Germano subgrid-scale closure method, *Physics of Fluids A*. 4 (3) (1992) 633‐636.

[43] Ansys, Ansys Fluent, 14.0 Theory guide, ANSYS, Inc., (2011)

[44] S. E. Kim, Large eddy simulation using unstructured meshes and dynamic subgrid-scale turbulence models, AIAA Paper (2004) 2004-2548.

[45] F. Durst, S. Ray, B. Unsal and O.A. Bayoumi, The development lengths of laminar pipe and channel flows, Journal of Fluids Engineering, 127(6) (2005) 1154‐1160.

[46] Y.Wang, K. Zhong, N. Zhang, and Y. Kang, Numerical analysis of solar radiation effects on flowpatterns in street canyons,Eng. Appl. Comput. Fluid Mech. 8(2) (2014) 252‐262.

[47] K. McGrattan, S. Hostikka, J. Floyd, G. Forney, T. Korhonen, and R. McDermott, Fire Dynamics Simulator (Ver. 6), Technical Reference Guide, NIST Special Publication Vol. 1018 NIST, (2012).

[48] M. Piirto, A. Karvinen, H. Ahlstedt, P. Saarenrinne, R. Karvinen, PIV measurements in square backward-facing step, Journal of Fluids Engineering 129 (2007) 984-990.

[49] J. Tihon, V. Penkavova, J. Havlica, M. Šimcik, The transitional backward-facing step flow in a water channel with variable expansion geometry, Experimental Thermal and Fluid Science 40 (2012) 112‑125.

[50] C. Schram, P. Rambaud, M. L. Riethmuller Wavelet based eddy structure eduction from a backward facing step flow investigated using particle image velocimetry, Experiments in Fluids 36 (2004) 233–245.

[51] J. C. Vogel and J. K. Eaton , Combined Heat Transfer and Fluid Dynamic Measurements Downstream of a Backward-Facing Step, J. Heat Transfer 107(4) (1985) 922-929.

[52] S. Yamada, H. Nakamura Spatial correlation of velocity and heat transfer downstream of a backward facing step using 2D-3C piv and IR thermography, International symposium on turbulence and shear flow Phenomena (TSFP-9) June 30-July 3, (2015), Melbourne, Australia

[53] G. L. Juste, E. M. Benavides, Moiré-Fourier deflectometry for local heat transfer measurement over a backward-facing step, International Journal of Thermal Sciences 77 (2014) 244-251.

[54] O. Kafri, I. Glatt, The physics of Moire´ metrology. New York: John Wiley and Sons; (1990). [Chapter 6, p.89‑109; Chapter 7].

[55] D. Naylor, A.D. Machin, The accuracy of beam-averaged interferometric temperature. Measurements in a three-dimensional field. Experimental Heat Transfer 14 (2001) 217‑228.

[56] V. Sajith, C.B. Sobhan, Digital interferometric measurement of forced convection heat transfer in a miniature rectangular channel, Exp. Heat Transfer 21 (2008) 314-333

[57] G.L. Juste, E.M. Benavides, End-wall errors in temperature measurement of external convective heat transfer with Moiré deflectometry, Optics and Lasers in Engineering 49 (2011) 8‑12.

[58] E. Keren, O. Kafri, Diffraction effects in Moiré deflectometry. Journal of the Optical Society of America A 2(2) (1985) 111‑120.

[59] E. Bar-Ziv Effect of diffraction on the Moire´ image. Journal of the Optical Society of America A 2(3) (1985) 380-385.

[60] S. Nicola, P. Ferraro, I. Gurov, R. Koviazin, M. Volkov, Fringe analysis for Moiré interferometry by modification of the local intensity histogram and use of a two-dimensional Fourier transform method, Meas. Sci. Technol. 11 (2000) 1328-1334.

[61] M. Hirp, P. Reitere, IDEA: Software for interferometrical data evaluation, Institut für Experimental Physik Technische, Universität Graz, Graz, Austria, (1999).

[62] R.J. Moffat, Describing the Uncertainties in Experimental Results, *Experimental Thermal Fluid Sciences*, 1, (1988) pp. 3-17.

[63] M. Ahmadi and K. Madanipour, Investigation of phase object trace duplication in moiré deflectometry, Applied optics, 55 (36) (2016), 10370-10374

[64] J. Jeong and F. Hussain, On the identification of a vortex, J. Fluid Mech. 285 (1995) 69‑94.

[65] V. Kolár, Vortex identification: new requirements and limitations, International Journal of Heat and Fluid Flow 28 (2007) 638‑652.